

PCCP

Accepted Manuscript



This is an *Accepted Manuscript*, which has been through the Royal Society of Chemistry peer review process and has been accepted for publication.

Accepted Manuscripts are published online shortly after acceptance, before technical editing, formatting and proof reading. Using this free service, authors can make their results available to the community, in citable form, before we publish the edited article. We will replace this *Accepted Manuscript* with the edited and formatted *Advance Article* as soon as it is available.

You can find more information about *Accepted Manuscripts* in the [Information for Authors](#).

Please note that technical editing may introduce minor changes to the text and/or graphics, which may alter content. The journal's standard [Terms & Conditions](#) and the [Ethical guidelines](#) still apply. In no event shall the Royal Society of Chemistry be held responsible for any errors or omissions in this *Accepted Manuscript* or any consequences arising from the use of any information it contains.

Unravelling the Impact of Hydrocarbon Structure on the Fumarate Addition Mechanism – a gas-phase *ab-initio* study.

Vivek S. Bharadwaj[‡], Shubham Vyas^{‡, #}, Stephanie M. Villano[‡], C. Mark Maupin[‡], and Anthony M. Dean^{‡ *}

[‡]Chemical and Biological Engineering Department, Colorado School of Mines, 1500 Illinois Street, Golden, CO 80401

[#]Department of Chemistry and Geochemistry, Colorado School of Mines, 1500 Illinois Street, Golden CO 80401

Corresponding Author

* To whom correspondence should be addressed: AMD, email: amdean@mines.edu, PHONE: 303-273-3643, FAX: 303-273-3730;

Funding Sources

ONR MURI Grant N00014-10-1-0946

KEYWORDS: Anaerobic Hydrocarbon Biodegradation, CHEMKIN, Glycyl Radical Enzyme, H-abstraction, Non-covalent Interactions, Stereo-preference.

ABSTRACT:

The fumarate addition reaction mechanism is central to the anaerobic biodegradation pathway of various hydrocarbons, both aromatic (e.g., toluene, ethyl benzene) and aliphatic (e.g., *n*-hexane, dodecane). Succinate synthase enzymes, which belong to the glycyl radical enzyme family, are the main facilitators of these biochemical reactions. The overall catalytic mechanism that converts hydrocarbons to a succinate molecule involves three steps: 1) initial H-abstraction from the hydrocarbon by the radical enzyme, 2) addition of the resulting hydrocarbon radical to fumarate, and 3) hydrogen abstraction by the addition product to regenerate the radical enzyme. Since the biodegradation of hydrocarbon fuels via the fumarate addition mechanism is linked to bio-corrosion, an improved understanding of this reaction is imperative to our efforts of predicting the susceptibility of proposed alternative fuels to biodegradation. An improved understanding of the fuel biodegradation process also has the potential to benefit bioremediation. In this study, we consider model aromatic (toluene) and aliphatic (butane) compounds to evaluate the impact of hydrocarbon structure on the energetics and kinetics of the fumarate addition mechanism by means of high level *ab-initio* gas-phase calculations. We predict that the rate of toluene degradation is ~100 times faster than butane at 298K, and that the first abstraction step is kinetically significant for both hydrocarbons, which is consistent with deuterium isotope effect studies on toluene degradation. The detailed computations also show that the predicted stereo-chemical preference of the succinate products for both toluene and butane are due to the differences in the radical addition rate constants for the various isomers. The computational and kinetic modeling work presented here demonstrates the importance of considering pre-reaction and product complexes in order to accurately treat gas phase systems that involve intra and inter-molecular non-covalent interactions.

1. Introduction

Biodegradation of hydrocarbons via anaerobic metabolic pathways provides a carbon source for microorganisms,¹⁻⁵ which enables the growth of microbial cultures, and results in significant microbial induced corrosion of fuel storage and transportation infrastructure.⁶⁻⁸ Fumarate addition is the first step in this anaerobic metabolic pathway and is catalyzed by enzymes of the succinate synthase family.^{4, 9} The fumarate addition reaction was first observed in toluene degrading bacterial cultures and led to the discovery of the Benzylsuccinate synthase (BSS) enzyme that is responsible for enabling anaerobic toluene metabolism.¹⁰ Since then a number of related enzymes (Alkylsuccinate synthase (ASS) and Methylalkylsuccinate synthase (MAS)) that now constitute the succinate synthase enzyme family have been implicated in the biodegradation of various hydrocarbon fuels.^{11, 12} The succinate synthase enzymes are a subset of the glycy radical enzyme (GRE) family and utilize free radical chemistry to catalyze the addition of different hydrocarbon substrates to fumarate.^{5, 10, 12-14} The succinate synthase enzyme sub-family shares the characteristic glycine residue that harbors the radical center and the cysteine residue that conducts the catalytic reaction, which is a common motif found in GREs. The sensitivity of the glycy radical to the presence of oxygen has made the experimental investigation into the structure and kinetics of succinate synthase enzymes extremely challenging. This has led to a significant gap in our understanding of the fumarate addition mechanism at a molecular-level. In our effort to bridge this gap, we have successfully used a range of computational techniques to predict the structure of the catalytic subunit of BSS and provided insights into the active site and the specific enzyme substrate interactions that enable fumarate addition in the case of toluene.¹⁵ These predictions, including details of the active site, have been very recently confirmed

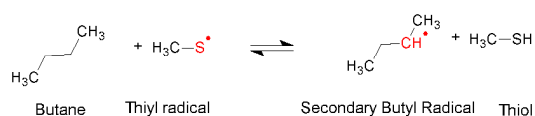
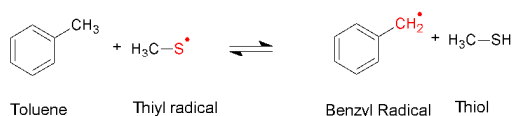
experimentally.¹⁶ Other investigations on succinate metabolites observed in bacterial cultures employing these enzymes have also shown the versatility of the fumarate addition mechanism in enabling the biodegradation of varied hydrocarbon fuel structures.^{14, 15, 17, 18} Understanding how hydrocarbon molecular structure impacts fumarate addition is hence, of utmost importance to the design of future fuels that are less susceptible to biodegradation and the associated bio-corrosion. Such understanding also has significant potential in advancing our ability to utilize anaerobic hydrocarbon metabolism as a suitable bioremediation strategy. A common computational technique for studying complex systems is to utilize reduced model gas-phase ab-initio studies, which have been crucial in providing first hand insights into several enzymatic mechanisms.¹⁹⁻²¹

The proposed reaction mechanism for fumarate addition is described via 3 steps, namely, the initial hydrogen abstraction, fumarate addition, and cysteine radical regeneration as shown in Scheme 1. The hydrogen abstraction step (Step 1) involves the generation of the hydrocarbon-based radical, which is generated through H-abstraction by the protein-based cysteine radical. This is followed by the addition of the hydrocarbon radical to fumaric acid (Step 2) to form the succinate radical intermediate. The final step involves the regeneration of the cysteine radical (Step 3) by hydrogen transfer from the cysteine residue to the succinate radical. In the enzyme, these three reactive steps are preceded by the generation of the glycy radical, and the docking of the substrate in the active site.¹⁵ This radical mediated mechanism is considered to be the mode of catalysis in all fumarate addition enzymes (BSS, ASS, MAS), which biodegrade different hydrocarbon substrates.^{5, 12}

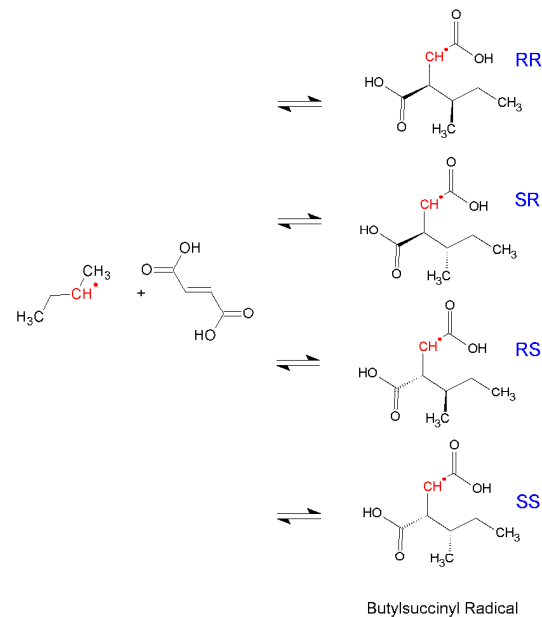
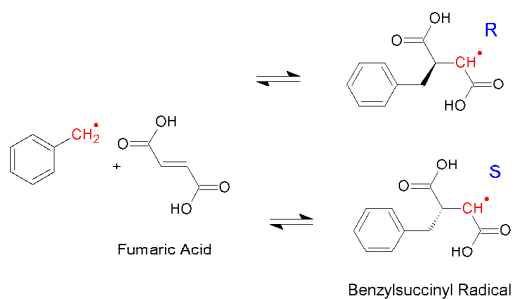
In this study, we evaluate the impact, in the gas phase, of hydrocarbon structure on fumarate addition by considering a model system consisting of fumaric acid, thiyl radical (representing the cysteinyl radical), and butane and toluene as model fuel species. These gas phase studies provide

underlying features of the potential energy surface without the impact of solvent and enzymatic effects, thus allowing us to evaluate the impact of hydrocarbon structure alone. We employ high-level electronic structure calculations to determine the potential energy surfaces for the three reactions involved in fumarate addition. The activation barriers and reaction thermodynamics are used to calculate rate constants for the reactions. The reactions are assembled into a kinetic model and the predictions of this model are a first step towards the ultimate goal of comparing predicted enzymatic fuel degradation rates with experimental fuel biodegradation rates. It is also of interest to note that the products of the enzymatic fumarate addition reaction, in case of both alkanes and aromatics, exhibit stereochemical preferences; for example, *R*-benzylsuccinate is the dominant isomer in the case of toluene degradation while *RR*-methyl-pentyl-succinate and *RS*-methyl-pentyl-succinate are the preferential products in the case of *n*-hexane degradation.^{17, 22} While the reason for this preferential stereochemistry has been attributed to the substrate dynamics in the enzyme active site,^{15, 22, 23} we explore the possibility of another basis for this stereo-preference by calculating the electronic structures for each stereoisomer and comparing their potential energy surfaces (Scheme 1, step 2 and 3).

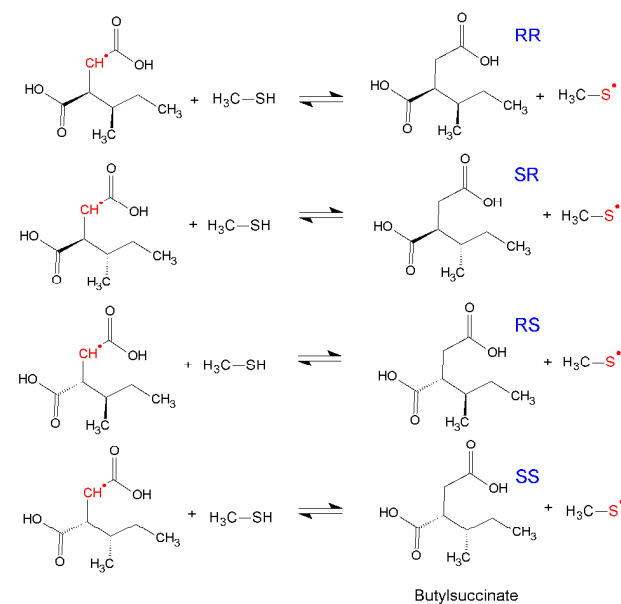
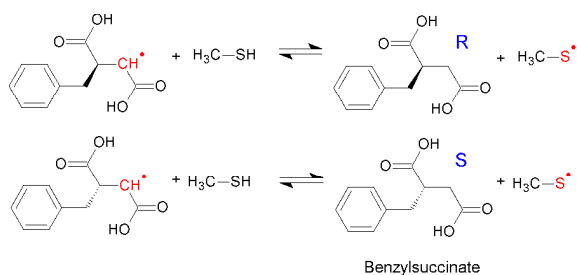
Step 1: Initial H-Abstraction



Step 2: Fumarate Addition



Step 3: Thiyl Radical Regeneration



Scheme 1: Steps involved in the fumarate addition mechanism for toluene (left) and butane (right). The radical centers involved in the reactions are shown in red and the stereo-isomers are colored blue. Fumarate addition in alkyl substrates is known to involve the sub-terminal carbon.²²

Electronic structure calculations on simplified enzyme systems have been successful at providing crucial insights into the specifics of enzymatic reaction mechanisms.²⁴⁻²⁸ In fact, calculations (at the B3LYP/6-31G(d,p) level of theory) by Himo *et al.* in 2002¹⁸, provided the first glimpse into toluene degradation via the fumarate catalytic mechanism in BSS. That study evaluated the potential energy surfaces for the different steps of the proposed mechanism and concluded that the fumarate addition step would be rate-limiting based on reaction barriers. This study computed only barriers and reaction enthalpies and did not attempt to compute reaction rate constants, which require evaluation of the pre-exponential factors by calculating differences in the entropies between the transition state and the reactants.

The discovery of the fumarate addition mechanism in the anaerobic biodegradation of saturated hydrocarbon substrates and the outstanding questions about the stereo-preferences and kinetics of the mechanism have prompted this re-evaluation of the fumarate addition mechanism using a more elaborate gas-phase quantum mechanics (QM) approach.^{17, 22, 29, 30} The availability of improved computational resources and methods enable a more accurate specification of the PES. The calculations outlined in this study reveal the importance of considering the impact of non-covalent interactions that lead to the formation of reactant and product complexes; these markedly affect the kinetics in this catalytic cycle. It is anticipated that these types of interactions within the active site of the enzyme will similarly impact the fumarate addition mechanism in the enzyme active site.

2. Methods

2.1 *Ab-initio* Calculations.

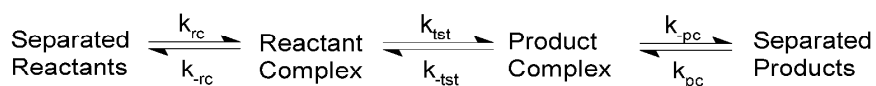
The potential energy surfaces (PES) for the fumarate addition mechanism were derived for toluene and butane for each of the three reactions (initial H-abstraction, fumarate addition and

thiyl radical regeneration) (Scheme 1). For the fumarate addition and thiyl radical regeneration steps, the PESs of all possible stereo-isomers of the succinate product; 2 for toluene (1 chiral center) and 4 for butane (2 chiral centers) were obtained. In the case of butane, the first letter indicates stereo-specificity of the chiral center on the alkane, and the second indicates the fumaric acid chiral center. The presence of sulfur and oxygen atoms in this system offers opportunities for sufficiently strong non-covalent interactions that can impact the kinetics at ambient temperatures. In order to account for this, post- and pre-reaction complexes were obtained based on intrinsic reaction coordinate (IRC) calculations from the transition state.³¹ The work-flow of the geometry optimization procedure is illustrated in Supplementary Information Scheme 1. The geometries of all molecular species (i.e. reactants, products, and transition states) were optimized independently and dihedral scans performed on all species to ensure that they are at their global minima. The scans for each dihedral on each transition state entailed a total of over 250 independent calculations and were performed at the M062X/6-31G level of theory. The IRC calculations were then performed on the lowest energy transition state conformer. Frequency calculations were performed to determine the nature of saddle points (i.e. transition states) and reactant/product minima (characterized by no imaginary frequencies). All calculations were performed using the Gaussian 09 computational package at the M06-2X density functional and the CBSB7 (6-311G(2d,d,p)) basis set.³²⁻³⁴ The M06-2X is a recent hybrid meta functional that incorporates significant Hartree-Fock exchange; is well known for accurate calculations for main group chemistry as well as accounting for non-covalent interactions and is widely regarded as the best replacement for B3LYP density functional.³⁵⁻³⁹ While the correct description of reactive systems might require a multi reference method, the relatively large nature (14 heavy atoms) of the complexes makes this approach computationally intractable.

M06-2X has been benchmarked against multi-reference methods⁴⁰ and has been shown to be accurate for predicting transition states,⁴¹ the treatment of general thermochemistry and kinetics^{35, 40} as well as thermochemistry of H-transfer reactions⁴². Due to the lack of scaling factors for the M60-2X level and the CBSB7 basis set, the frequencies were not scaled. The complex nature of the potential energy surface in the 3-D configurational space of these systems precluded the evaluation of hindered rotor potentials. Since the contribution from hindered rotors are roughly equivalent in the reactants/products and the transition state, due to the relatively simple nature of the reactions (H-abstractions and addition reactions) in this mechanism, the impact of the neglecting hindered rotors is considered to be minimal.

2.2 Kinetic Modeling.

A total of 14 potential energy surfaces, including 4 stereoisomers for butane and 2 stereoisomers for toluene, were computed. Each reaction was treated as a sub-mechanism consisting of 3 steps; reactant complex (RC) formation, transition state (TS) crossing and product separation (Scheme 3). The following are the rate constants involved in the sub-mechanism k_{rc} , k_{-rc} , k_{tst} , k_{-tst} , k_{pc} and k_{-pc} .



Scheme 3: Reaction sub-mechanism and its associated rate-constants.

The rate constants, k_{rc} and k_{pc} are calculated based on collision theory using the formula:

$$k_{rc} = k_{coll} = \frac{\pi d_{coll}^2}{\sigma_{AB}} \sqrt{\frac{8k_B T}{\pi\mu}} \quad (1)$$

Here d_{coll} is the collision diameter (assumed to be 4 Å), σ_{AB} is the symmetry factor, (unity in all cases considered here), k_{B} is the Boltzmann constant, T is the temperature and μ is the reduced mass of the two colliding species.

Rate constants for the transition state (TS) crossing, k_{tst} were calculated based on transition state theory according to the following formula utilizing the activation barriers computed by the aforementioned gas phase quantum mechanical calculations:

$$k_{\text{tst}} = A \exp \frac{-E_a}{RT} \quad (2)$$

The pre-exponential factor A was calculated using:

$$A = \frac{k_{\text{B}}T}{h} \exp^{(1-\Delta n^\ddagger)} \exp \frac{\Delta S^\ddagger}{R} \quad (3)$$

where h is the Planck's constant, Δn^\ddagger and ΔS^\ddagger are the change in the number of species and entropy, respectively, between the transition state and the reactant complex. The activation energy E_a is calculated using eq. 4 and the thermochemistry data from the computations described in section 2.1:

$$E_a = \Delta H^\ddagger + (1 - \Delta n^\ddagger)RT \quad (4)$$

where ΔH^\ddagger is the enthalpy difference between the transition state and the reactant complex as obtained by the gas phase calculations. The tunneling factors for hydrogen transfer steps were calculated using the Wigner formula and were found to be small (~20%) for both toluene and butane.⁴³ These are not included in the analysis.

The reverse rate constants for reactant complex (RC) formation ($k_{\text{-rc}}$), reaction ($k_{\text{-tst}}$) and product separation ($k_{\text{-pc}}$) are calculated based on the equilibrium constants for the respective reactions.

$$K_{\text{eq}} = \exp \frac{-\Delta G_{\text{rxn}}}{RT} (RT)^{\Delta n} \quad (5)$$

and

$$k_{rev} = \frac{k_{forw}}{K_{eq}} \quad (6)$$

where R is the universal gas constant, ΔG_{rxn} and Δn are the free energy differences and change in the number of moles between products and reactants respectively.

The rate constants for each step of the three-step fumarate addition mechanism (Scheme 1) for each stereoisomer of toluene and butane resulted in a total of 72 reactions (toluene-26 and butane-46) with 41 species (toluene-14, butane-24 and common-3). CHEMKIN-PRO ver. 15131 was used for kinetic modelling and analysis.⁴⁴ The sensitivity coefficients are calculated by using logarithmic sensitivity gradients,

$$S_i = \frac{\partial \log F}{\partial \log \alpha_i} \quad (7)$$

where F is the observable (the concentration of a particular species at a specific time) and α_i is the parameter that is varied (the A-factor for a reaction rate constant).

In general the formation of reactant and product complexes in this system could be considered as a chemically activated reaction with pressure-dependent rate constants due to the competition between dissociation, stabilization, and reaction of the initially-formed energized adduct. In this study, high-pressure rate constants were considered since the enzyme catalyzed fumarate addition reaction takes place in the condensed phase and therefore the rate constants are expected to be at the high-pressure limit.

3. Results and Discussion

3.1 Potential Energy Surfaces

3.1.1 Initial H-Abstraction

The PESs computed for the first step of the mechanism reveal differences between benzyl and butyl radical formation as shown in Figure 1. Since this step involves the cleavage of a C-H bond and the formation of an S-H bond, the difference in the overall ΔH_{rxn} , (i.e., $\Delta\Delta H_{\text{rxn}}$) for butane and toluene should be comparable to the difference in their bond dissociation energies. Our calculations indicate a $\Delta\Delta H_{\text{rxn}}^{\text{butane-toluene}}$ of 7.8 kcal/mol while the experimentally measured difference in bond dissociation energies for $\text{CH}_3\text{CH}_2(\text{CH}_3)\text{CH-H}$ and $\text{C}_6\text{H}_5\text{CH}_2\text{-H}$ is 8.4 ± 0.8 kcal/mol,⁴⁵ verifying the accuracy of the computational protocol employed in this study. Considering only separated reactants (and products) for toluene, Himo and coworkers estimated the ΔH_{rxn} to be 3.4 kcal/mol and the barrier to be 10.7 kcal/mol,¹⁸ whereas this study reveals the ΔH_{rxn} to be 4.5 kcal/mol and the barrier to be 7.8 kcal/mol. The differences in reaction enthalpies and reaction barriers are attributed to the use of different levels of theory.

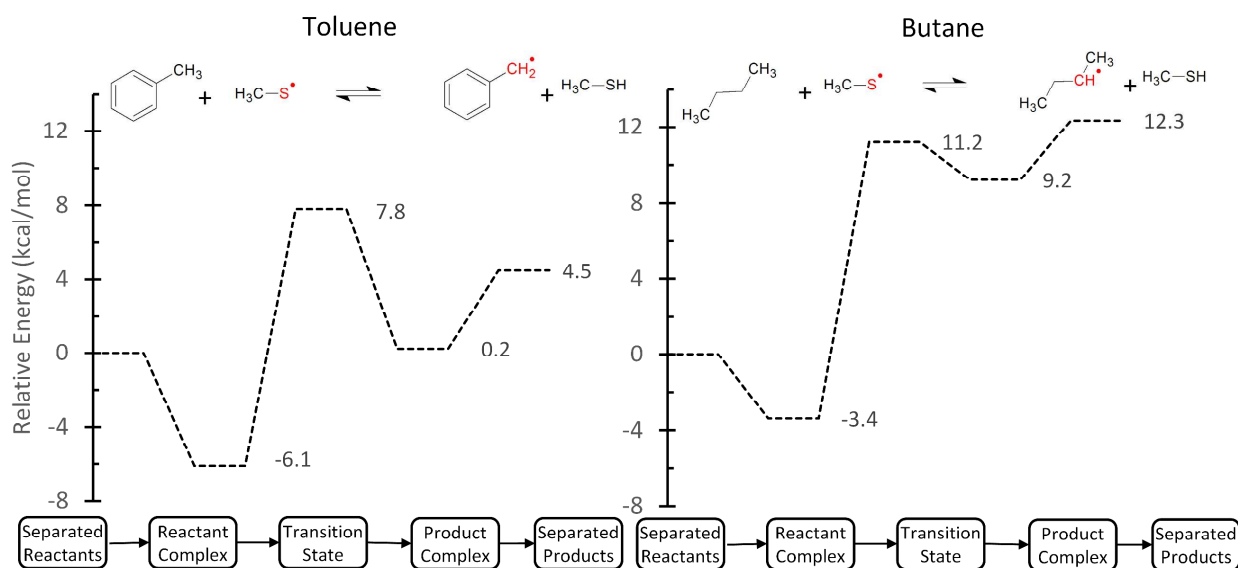


Figure 1: Potential energy surfaces for the first step (initial H-abstraction) of fumarate addition in the case of toluene (left) and butane (right). The schematic (inset) indicates the sub-mechanism for reaction progress in the presence of reactant and product complexes.

The significance of fuel structure and its impact on the fumarate addition mechanism is immediately evident upon comparison of the energies of reactant and product complexes for butane and toluene. For the reactant complex, the stabilization energy in the case of toluene is almost 2.7 kcal/mol greater than in the case of butane (i.e., 6.1 kcal/mol vs. 3.4 kcal/mol). This is attributed to the favorable interactions between the π -electron cloud of toluene and the methyl group of the thiol, which stabilizes the toluene complex and is absent in the butane complex. The common factor that stabilizes both reactant complexes is observed to be the non-covalent interactions of the sulfur atom with hydrogens on the hydrocarbons (Supplementary Information Figure S1). A comparative analysis of the spin density distributions, utilizing Mulliken spin density, between the reactant and product complexes in the case of the toluene indicates that 26% of the spin density from the sulfur radical is shared amongst carbons of the aromatic ring in the product complex, while in the case of butane, only 3% spin is shared amongst the other alkyl carbons in the product (Supplementary Information Section S1.1) The increased spin density delocalization in the case of toluene is indicative of resonance and hence accounts for a high degree of stabilization. The implications of the difference in stabilization between toluene and butane on the fumarate addition mechanism are discussed in more detail in the kinetic modeling section.

3.1.2 Fumarate addition

It is known that in nature, the fumarate addition mechanism is stereo-preferential, as observed in the anaerobic biodegradation of toluene where *R*-benzylsuccinate was found to be the predominant isomer.¹⁷ More recently, it has also been observed that anaerobic biodegradation of *n*-hexane yields only the *RR* and *RS* stereoisomers of the resulting methyl-pentyl-succinate product.²² These experimental findings indicate that the mode of action for the fumarate addition

step plays an important role in determining the stereo-preference of the resulting product(s). Hence, separate PESs for each stereoisomer were investigated for this step of the mechanism.

Although the reactant complexes in both butane and toluene are similarly stabilized (Figure 2), the barrier for addition in the case of toluene (~ 6.5 kcal/mol) is significantly higher than butane (~ 1.5 kcal/mol). This difference is consistent with literature on carbon radical addition where the difference in activation energies for benzyl radical addition (10.9 kcal/mol) and secondary propyl radical addition (5.3 kcal/mol) to ethene is ~ 5.4 kcal/mol.⁴⁶ This difference is attributed to the loss of resonance stabilization in the benzyl radical. Considering the infinitely separated reactants and product, the ΔH_{rxn} and activation barrier for toluene in the current study is around 10 kcal/mol lower (ΔH_{rxn} : ~ -21 vs. -10 kcal/mol; E_a : ~ 0 vs. 8.5 kcal/mol) when compared to previously published results.¹⁸ This is attributed to the differences in the level of theory utilized, specifically the accounting of non-covalent interactions at the M06-2X level.

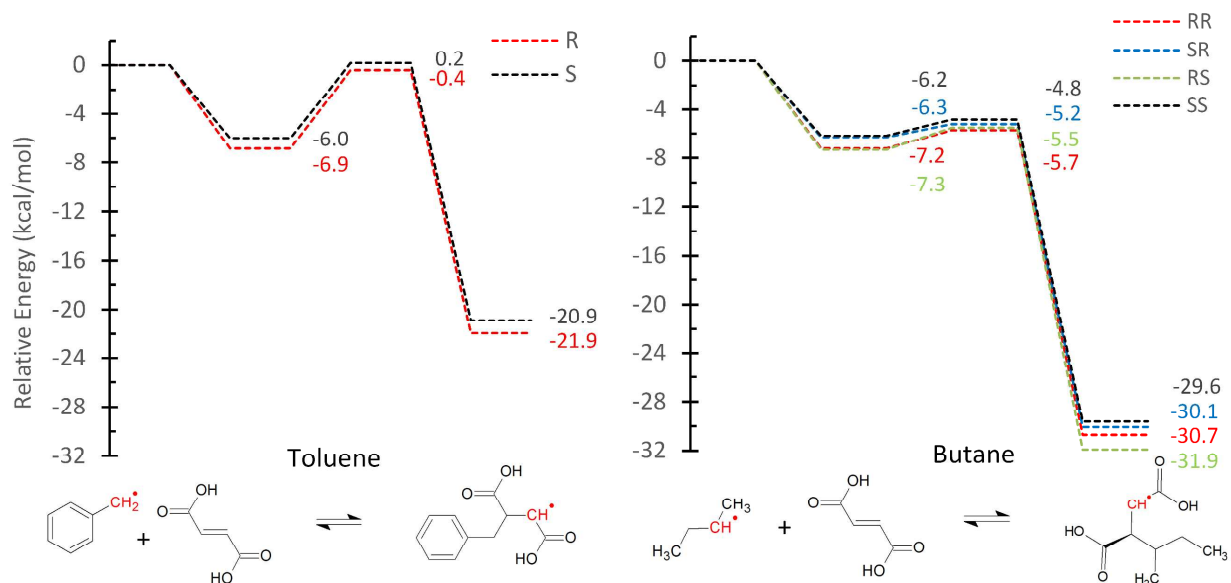


Figure 2: Potential energy surfaces for the second step (i.e. fumarate addition) in the case of toluene (left) and butane (right). For toluene the PES of for stereoisomers *R*-benzylsuccinate is shown in red and *S*-benzylsuccinate is shown in black. For butane, the color scheme for the succinate stereoisomers is *RR* - red, *SR* - blue, *RS* - green and *SS* - black.

Amongst the stereoisomers for toluene, the PES corresponding to the *R* stereoisomer is slightly more stabilized than that of the *S* stereoisomer while in the case of butane, the *RS* and *RR* isomers are slightly lower in energy than the *SS* and *SR* isomers. In this fumarate addition step, the exothermicity arises from the fact that a C=C double bond is converted to a C-C single bond and another C-C single bond is formed. It is observed that the ΔH_{rxn} in the case of butane is ~ 9 kcal/mol more exothermic than in the case of toluene, which is attributed to the loss of resonance stabilization of the benzyl radical.

3.1.3 CH_3S regeneration

The third step of the mechanism involves the hydrogen atom transfer from thiol to the succinate radical to yield the succinate product and regenerate the thiyl radical for subsequent reaction. The stabilization of the reactant complexes, the barriers for the reaction as well as the reaction enthalpies (ΔH_{rxn}) for butane and toluene are very similar, unlike the first two steps of the mechanism (Figure 3). This is not surprising considering the fact that for the CH_3S regeneration step, the reactive center is on the fumaric acid portion of the succinate radical and hence there is almost no impact of the hydrocarbon fuel structure on this step. Comparison of calculated results in Figure 3 with previous work by Himo *et al.* shows a relatively lower activation barrier (7 vs. ~ 3 kcal/mol, relative to the infinitely separated reactants) and a more exothermic reaction for CH_3S regeneration ΔH_{rxn} (-5.8 vs. -7 kcal/mol) in this study.¹⁸ Amongst the stereo-isomers of toluene, *R*-benzylsuccinate is relatively more stabilized at all stages of the reaction as compared to *S*-benzylsuccinate, which is similar to what was observed for Step 2. In the case of butane, one can observe differences in the stabilization of reactant and product

complexes amongst isomers, which are attributed to the specific non-covalent interactions that arise due to the different geometries in each case, although there seems to be no particular trend in the stabilization amongst the isomers.

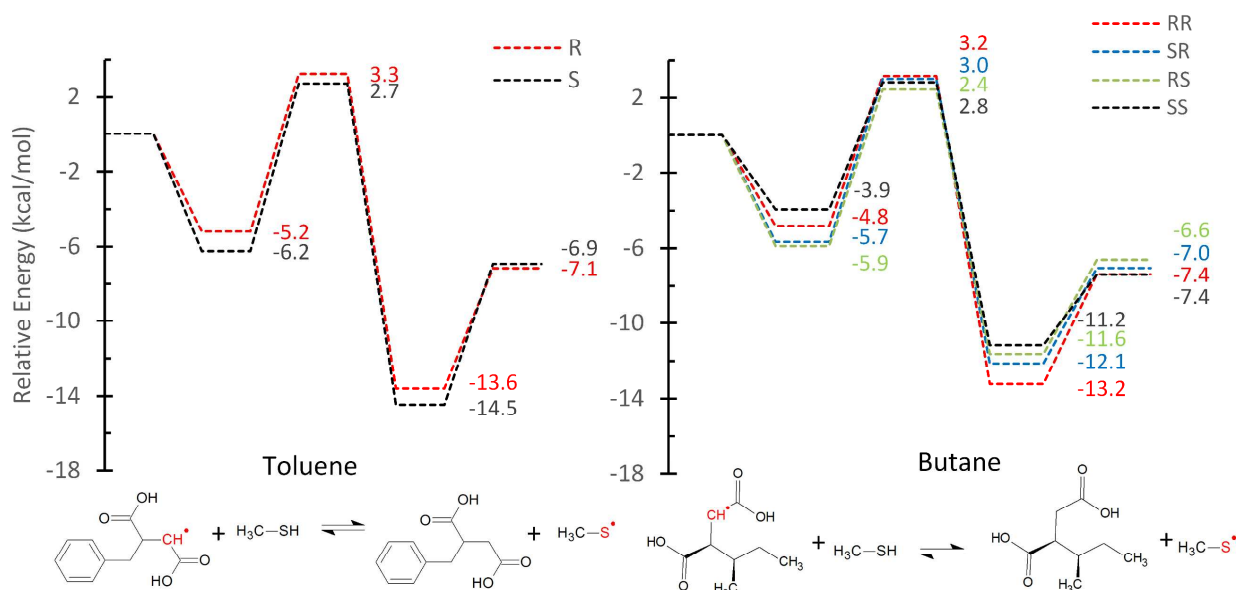


Figure 3: Potential energy surfaces for the third step (i.e. CH₃S regeneration) in the case of toluene (left) and butane (right). For toluene the PES of for stereoisomers *R*-benzylsuccinate is shown in red and *S*-benzylsuccinate is shown in black. For butane, the color scheme for the succinate stereoisomers is *RR* - red, *SR* - blue, *RS* - green and *SS* - black.

3.2 Kinetic Modeling

While the PESs provide insight into the energetics (reaction enthalpies and reaction barriers) of fumarate addition, this is only a part of the overall picture. The electronic structure calculations allow us to use statistical mechanics to calculate reaction entropies and free energies for the reactions involved in this mechanism. Hence the next step towards understanding the impact of hydrocarbon structure on the fumarate addition reaction is to calculate the rate constants associated with the various parts of the mechanism using the thermodynamic quantities obtained from the electronic structure calculations as inputs for reaction rate theory. The derived rate constants (i.e. k_{rc} , k_{-rc} , k_{tst} , k_{-tst} , k_{pc} and k_{-pc}) for the complete mechanism at 298 K for toluene and

butane are listed in Table 1. The comprehensive list of reactions, their associated A-factors and activation barriers are listed in Table S3 of the Supplementary Information. In order to have a kinetic model that is representative (to a certain extent) of the enzyme system, we chose initial mole fractions of 0.18% for the hydrocarbon and fumaric acid, 72 ppm for the thiyl radical and the remainder to be an inert gas Ar (99.63%). A pressure of 1000 atm (representative of the condensed phase) and a temperature of 298 K were used in a closed homogenous batch reactor. The reactions were allowed to progress until the hydrocarbon (i.e. toluene or butane) concentrations were negligible and the final succinate products concentrations were constant.

Table 1: The set of rate constants that constitute the reaction mechanism for toluene and butane at 298K.

	k_{rc} ($\text{cm}^3/\text{mol}\cdot\text{s}$)	k_{-rc} (sec^{-1})	k_{tst} (sec^{-1})	k_{-tst} (sec^{-1})	k_{-pc} (sec^{-1})	k_{pc} ($\text{cm}^3/\text{mol}\cdot\text{s}$)
Step 1	Initial H-abstraction					
Toluene	1.36E+14	2.81E+12	4.27E+01	2.26E+07	5.17E+14	1.36E+14
Butane	1.49E+14	5.88E+13	4.42E+00	2.06E+09	4.63E+14	1.49E+14
Step 2	Fumarate Addition					
Toluene R	1.06E+14	4.80E+11	6.66E+05	5.78E-04		
Toluene S	1.06E+14	1.49E+13	1.72E+07	2.36E-03		
Butane RR	1.23E+14	1.00E+13	1.04E+10	2.16E-05		
Butane RS	1.23E+14	3.05E+12	2.38E+09	1.03E-06		
Butane SR	1.23E+14	3.69E+13	6.96E+09	1.33E-05		
Butane SS	1.23E+14	6.27E+13	6.51E+09	1.27E-05		
Step 3	Thiyl Radical Regeneration					
Toluene R	1.22E+14	1.73E+14	1.62E+05	8.60E-02	1.14E+13	1.23E+14
Toluene S	1.22E+14	3.09E+14	7.11E+06	1.61E-01	5.20E+11	1.23E+14
Butane RR	1.24E+14	5.45E+12	3.08E+04	6.94E-01	1.24E+13	1.25E+14
Butane RS	1.24E+14	7.33E+12	1.12E+05	3.95E+00	5.88E+12	1.25E+14
Butane SR	1.24E+14	1.57E+12	1.34E+06	1.32E+02	5.58E+13	1.25E+14
Butane SS	1.24E+14	4.63E+13	5.59E+05	3.75E+01	2.30E+14	1.25E+14

An important aspect of this study is the impact of the formation of reactant and product complexes. While we have seen how these complexes modify reaction barriers, a closer look at some of the TS crossing rate constants (k_{tst}) offers an indication of how complexes impact reaction kinetics. For example, in the initial H-abstraction step, if we were to ignore the presence of complexes and consider just the separated reactants and products, we have toluene being less endothermic than butane by 7.8 kcal/mol. If this difference correlated with the difference in activation energies, $k_{\text{tst}}^{\text{Toluene}}$ would be $>10^5$ times greater than $k_{\text{tst}}^{\text{Butane}}$, assuming an Evans-Polanyi factor of 0.6. This is in contrast to our result that $k_{\text{tst}}^{\text{Toluene}}$ is only ~ 10 times $k_{\text{tst}}^{\text{Butane}}$. This difference is due to the deeper well for the reactant complex in the H-abstraction step for toluene, which almost equalizes the barriers for TS crossing between toluene and butane. Another interesting outcome of considering complexes is the fact that since they are the only gateway to TS crossing, their thermodynamics significantly impacts the overall kinetics of the mechanism. The ensuing kinetic analyses extend these insights and are discussed in the context of the comparative degradation rates for toluene and butane in the gas phase, the kinetically significant step(s) for the mechanism, and a plausible basis for the observed stereo-preference of the fumarate addition reaction.

3.2.1 Overall hydrocarbon degradation rates

One of the primary goals of this kinetic analysis is to compare the relative rates of fumarate addition (or fuel degradation) between aliphatic and aromatic fuels. Figure 4 compares the predicted time evolution of fuel degradation between the butane and toluene systems. It is apparent that toluene degrades much faster than butane, requiring only ~ 210 s for 50% conversion while butane requires $\sim 22,000$ s for the same conversion. It is also predicted, in the case of butane, that the thiyl radical concentration reaches steady state almost immediately, thus

enabling one to treat the kinetics of fuel decay as a pseudo first order reaction. The pseudo first order rate constant for butane is calculated to be $3.2 \times 10^{-5} \text{ s}^{-1}$ at 25°C . In the case of toluene, it takes longer to approach pseudo first order kinetics due to the time required for the CH_3S concentration to achieve steady state (Figure 4). We obtained an approximate pseudo first order rate constant for toluene (0 to 75% conversion) by fitting the semilog slope to obtain a value of $3.17 \times 10^{-3} \text{ s}^{-1}$, approximately 100 times faster than butane. The predicted pseudo first order kinetics for toluene decay are consistent with that observed experimentally; however, a comparison of actual rate constants would not be appropriate since the rate constant depends on the thiyl radical concentration, which is assigned an arbitrary value in this study and was not determined experimentally.⁴⁷

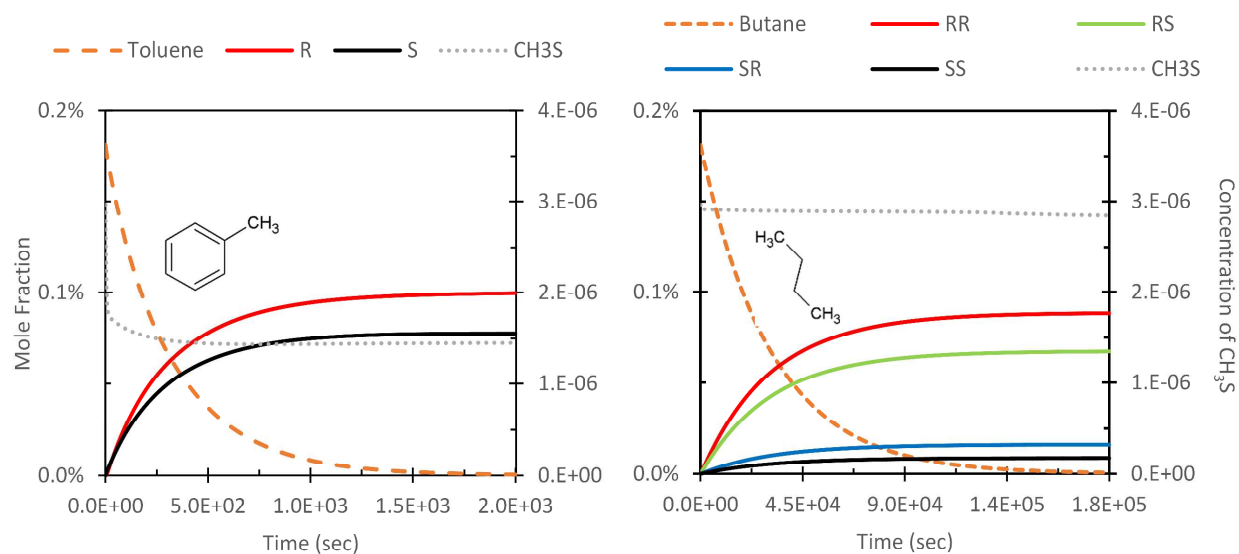


Figure 4: Overall degradation rates for toluene (left) and butane (right). Note the time scales for butane and toluene are different. The hydrocarbon mole fractions (left axis) are represented as a dashed line (brown) and the thiyl radical CH_3S concentrations (right axis) as a dotted line (gray) in each case. For toluene the generation of the two stereoisomers is shown in red (*R*-benzylsuccinate) and black (*S*-benzylsuccinate). For butane the color scheme for the stereoisomers is *RR* - red, *SR* - blue, *RS* - green and *SS* - black.

3.2.2 Rate controlling reactions

Himo *et al.* proposed the rate limiting step of the mechanism to be the fumarate addition step based on the reaction enthalpies and the overall barrier for the toluene reaction mechanism.¹⁸ However, in that study rate coefficients were not evaluated, and hence no explicit kinetic calculations were performed. The kinetic model developed in this study allows us to perform a sensitivity analysis on the reactions in the mechanism to identify the kinetically significant step(s). The sensitivity analysis is insightful since it quantifies the impact of different reactions on the production or consumption of a particular species, even though the reaction itself might not involve that species. In this study, each step of the mechanism has the corresponding forward and reverse reactions included explicitly with the respective rate constants satisfying microscopic reversibility to assure thermodynamic consistency. The advantage of this approach is that it enables the sensitivity analysis to identify reactions that might be partially equilibrated; if such a reaction is important, it will show up with large sensitivity coefficients, but with opposite signs for the forward and reverse directions. For such a case, the appropriate conclusion is that the reacting system is sensitive to the thermodynamics of the reaction, i.e., it is the ratio of k_{forw} and k_{rev} rather than the individual rate constants that affect the rate. Alternatively, if we were to only specify the forward rate constant and let the program determine the reverse rate constant based on microscopic reversibility, an increase in the forward rate would result in an increase in the reverse rate (since the equilibrium constant remains unchanged) and the impact of the equilibrium constant on the kinetics would remain hidden.

Figure 5 illustrates the important reactions of the mechanism that impact hydrocarbon (i.e., toluene and butane) concentration. Since these sensitivities relate to the reactant, a negative value means that an increase in the rate constant increases the rate of reaction and hence the consumption of the reactant. Butane presents a relatively straightforward case with only 3

reactions being important, all of which involve the initial H-abstraction. Two of these are the forward and reverse rate constants for formation of the initial reactant complex (RC), and the third is the subsequent TS crossing from the RC. The symmetric positive and negative sensitivities for formation and dissociation of RC indicate this reaction is rapidly equilibrated, with the concentration of RC controlled by the equilibrium constant for this reaction. The sensitivity of the TS crossing is identical to the formation of RC. This indicates that two factors dictate butane degradation; the thermodynamic equilibrium that controls the concentration of RC and the TS crossing rate constant. These results suggest that butane conversion can be described as a second order reaction with rate constant $k_{reduced}^{butane} = K_{eq}^{RC} k_{ts} = 11.20 \frac{cm^3}{mol.s}$. Considering the steady-state concentration of the thiyl radical (Figure 4), the corresponding pseudo first order rate constant is $3.2 \times 10^{-5} s^{-1}$, consistent with that calculated in the previous section from the kinetic model predictions. Thus the hydrogen abstraction reaction step is rate limiting for butane degradation, and the formation of RC plays a critical role in the degradation process.

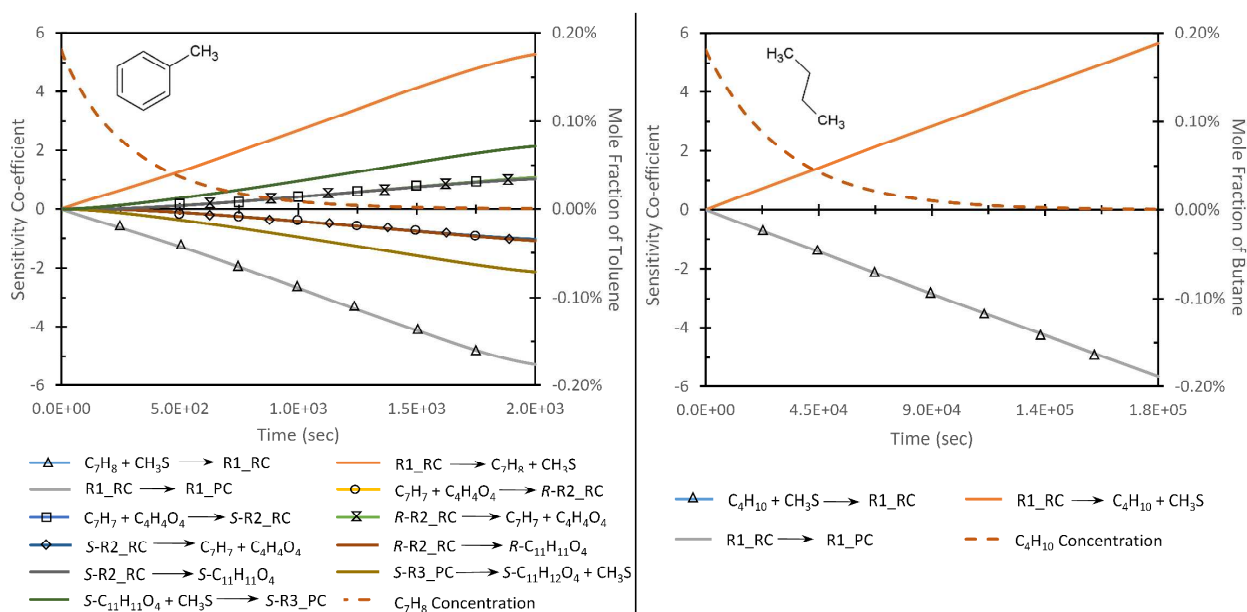


Figure 5: Results of the sensitivity analysis for toluene (left) and butane (right). The dashed lines on each graph represent the time evolution of hydrocarbon mole fraction. The time evolution of sensitivity co-efficients for important reactions that affect hydrocarbon mole fraction are indicated as color coded lines. It may be noted that the sensitivities for the TS crossing reaction and RC formation reaction for the H-abstraction step overlap in the case of butane. Similarly, for toluene, the sensitivities for the TS crossing reaction and RC formation reaction overlap for the H-abstraction and fumarate addition steps. The reactions that are not visible due to the overlap have been indicated with the symbols Δ , \square , \circ , \diamond and \otimes . Note: The time scales for toluene and butane are different.

In contrast to butane, the toluene sensitivity analysis suggests a more complex reaction network. Here all three steps of the mechanism turn up in the sensitivity analysis. As with butane, the reactions involved in the initial H-abstraction step are found to be kinetically the most significant (i.e. have the highest sensitivity coefficients), and both the equilibrium concentration of the RC and the hydrogen abstraction are important. The next largest set of sensitivity co-efficients belong to the three reactions (i.e. RC equilibrium followed by hydrogen abstraction) that involve the final hydrogen abstraction to regenerate the thiyl radical. The same sequence of reactions for the fumarate addition step show the smallest sensitivities to fuel degradation.

It is interesting to note that the non-constant thiyl radical concentration observed in toluene at earlier times (< 50% conversion) is a result of the thiyl radical being sequestered in the species involved in the fumarate addition and thiyl radical regeneration step and is consistent with the results of the sensitivity analysis. Hence the varying thiyl radical concentration during toluene degradation and the results of the sensitivity analysis for toluene make it difficult to compare the pseudo first order rate constants from the rate analysis and the reduced rate constant (i.e. $k_{reduced}^{toluene} = K_{eq}^{RC} k_{1st}$) as was done for butane. The fact that the initial H-abstraction step is kinetically significant in the case of toluene is consistent with experimental observations by Li *et al.*, who measured slower rates using deuterated toluene. If the fumarate addition were rate

H-abstraction, fumarate addition and the thiyl radical regeneration steps. The reactions that are not visible due to the overlap have been indicated with the symbols Δ , \square , \circ and \diamond . Note: The time scales for toluene and butane are different.

3.2.3 Differences between fumarate addition in alkanes & aromatics: Effects of reactant complexes

The role of hydrogen bonding in hydrogen abstraction reactions has recently been explored experimentally and computationally where it was found that triplet state hydrogen bonding could accelerate hydrogen abstraction reactions.⁴⁸ Here we consider the impact of hydrogen-bonded complexes on the fumarate addition reactions.

As discussed earlier, although the overall rate of toluene degradation is faster than butane, the difference is not as great as was expected based on the difference in reaction enthalpies for H-abstraction. This reduction of the anticipated impact of fuel structure in this study is caused by two factors. First, formation of the RC for the initial H-abstraction nearly equalizes the barriers for TS crossing. Offsetting this is the deeper well for the toluene RC (Figure 1), leading to a larger steady-state RC concentration and thus a faster rate. We might also have expected the lack of resonance stabilization in the product complex (PC) of butane to shift the equilibrium for the H-abstraction step towards the RC from the PC. However, this does not occur since the reaction product is promptly consumed in the further steps of the mechanism. Second, as revealed in the sensitivity analysis, the fumarate addition step is crucial to determining the rate of toluene degradation while it plays no significant role in butane degradation. This is consistent with the PESs (Figure 2) where the RCs are equally stabilized in both cases, but the TS crossing barrier is significantly higher for toluene as compared to butane.

Hence, even in the gas-phase, the predicted formation of hydrogen-bonded complexes significantly alters the expectations of the relative rates of fumarate addition between alkyl and aromatic fuel structures. The consideration of such complexes is also of particular relevance to understanding the mechanism in the enzymatic scenario. The presence of the protein backbone and functional amino acid side chains in the enzyme offers numerous avenues for reactant, TS, and product stabilization by hydrogen bonding, hydrophobic interactions and other non-covalent interactions at the active site¹⁵ that are likely to markedly affect the relative degradation rates for various hydrocarbon structures.

3.2.4 Possible basis for stereo-chemical preference in fumarate addition.

The experimentally observed stereo-preference for *R*-benzylsuccinate production from toluene has provided insights into the active site geometry in the enzyme for fumarate addition.^{17, 49} In the case of *n*-hexane degradation, the observation of the preference for *RS* and *RR* methyl-pentyl-succinates has suggested that inversion plays a crucial role in determining stereo-chemical preference and that the active site is primed to conduct the fumarate addition in a concerted manner.²²

The PESs described earlier show different energetics for the various stereoisomers, providing a potential explanation for stereo-bias, and the model predictions do exhibit stereo-bias in the isomers formed. However, the different predicted product distributions could be due to either differences in the overall equilibrium constants, due to slightly different thermodynamics properties of the isomer, or it could be due to kinetic effects. To differentiate these causes for stereo-preference, in Table 2 we compare the ratios of the stereoisomers predicted by the kinetic model to those expected if the products were formed in equilibrium amounts. The table lists the

free energy differences for the overall reaction, the corresponding equilibrium constants, the final concentrations predicted by the model and the reduced rate constant for the fumarate addition step (i.e., $k_{reduced}^{FA} = [K_{eq}^{RC} k_{1st}^{FA}]$) for all the succinate stereoisomers formed. The corresponding normalized entities are ratios of the specific quantity with that of the R isomer in the case of benzylsuccinate and the RR isomer in the case of butylsuccinate.

Table 2: Overall free energy differences, equilibrium constants, steady state concentrations of final products and reduced rate constants for the fumarate addition step.

	$\Delta G_{overall}^*$ [kcal/mol]	K_{eq}^{298} [cm ³ /mol]	Final product concentrations [mol/cm ³]	$k_{reduced}^{FA} = K_{eq}^{RC} k_{1st}$ [cm ³ /mol.s]	Normalized $K_{eq}^{298 \psi}$	Normalized concentrations	Normalized $k_{reduced}^{FA}$
Benzylsuccinate							
<i>R</i>	-11.8	1.10E+13	4.07E-5	1.47E+8	1.000	1.000	1.000
<i>S</i>	-10.6	1.34E+12	3.18E-5	1.22E+8	0.122	0.781	0.829
Butylsuccinate							
<i>RR</i>	-11.7	1.00E+13	3.61E-5	1.28E+11	1.000	1.000	1.000
<i>RS</i>	-12.5	3.54E+14	2.75E-5	9.60E+10	35.400	0.762	0.750
<i>SR</i>	-10.4	1.05E+12	6.61E-6	2.32E+10	0.105	0.183	0.181
<i>SS</i>	-10.5	1.25E+12	3.61E-6	1.28E+10	0.125	0.100	0.100

$$*\Delta G_{overall} = G_{succinate} - (G_{fumarate} + G_{toluene/butane})$$

ψ Normalized by the K_{eq}^{298} for R-Benzylsuccinate for toluene and RR-butylsuccinate for butane

In the case of toluene, note the predicted ratio from the kinetic model agrees very well with the ratio of rate constants for the benzyl addition step and differs significantly from that predicted at equilibrium, a clear indication that the preference is driven by the kinetics. The non-equilibrium product distribution can be understood by examination of the PES in Figure 3. Once the last hydrogen transfer occurs, the barrier for the reverse reaction is sufficiently high that the products are locked into the non-equilibrium distribution. It is interesting to note that for the enzyme catalyzed reaction, the experimentally observed ratio between the *R* and *S* isomers concentrations is 95:5 in favor of *R*, which is much closer to the equilibrium distribution of 89:11.

In the case of butane, the observed differences in final product concentrations of the stereo-isomers are more pronounced as compared to toluene with the steady-state concentrations of the final succinate products being in the following ratio 49:37:9:5 for the *RR*, *RS*, *SR* and *SS* isomers (Table 2). Despite *RS* being the thermodynamically most favorable stereo-isomer, the *RR* isomer is found to be the most favored based on steady state concentrations predicted by the model (Table 2). The results for butane parallel those for toluene in that the product distributions are driven by the kinetics. There is a good correlation of the ratio of model-predicted isomers with the ratio of rate constants for the butyl radical addition step, suggesting that the kinetics of fumarate addition step determines the stereo-bias observed in this study.

4. Conclusions

The gas-phase energetics governing the fumarate addition reaction mechanism and the impact of hydrocarbon structure have been evaluated using high level *ab initio* calculations and kinetic modeling. We have demonstrated that the formation of pre- and post-reaction complexes (due to the presence of S, O and H atoms) modify the potential energy landscape and have a significant impact on the reaction kinetics. At 298K, we predict the rate of degradation of toluene to be ~100 times faster than butane. Neglecting such complexes would lead to a much greater difference in the rates, reflecting the ~8 kcal/mol difference in C–H bond strengths. The results of the kinetic model have led us to revise the previous understanding of the mechanism by showing that the initial H-abstraction step, and not the fumarate addition step is an important rate-limiting step. This is also consistent with experimental observations of the deuterium isotope effects on toluene degradation in BSS.⁴⁷ The fuel degradation rate in the case of butane is found to be dictated by the formation of an equilibrated pre-reaction complex and the subsequent TS

crossing rate constant for the initial H-abstraction step. The observation of a steady state concentration for the thiyl radical allows butane degradation to be described by pseudo-first order kinetics. On the other hand, the initial H-abstraction, the thiyl radical regeneration as well as fumarate addition steps are found to be important for toluene degradation. We have shown that the predicted stereo-preference of fumarate addition is due to differing rate constants for the radical addition step for both fuels.

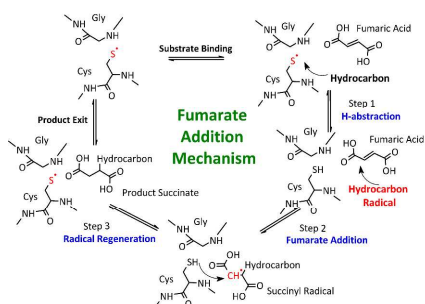
As evidenced throughout this study, the reactant complexes play an important role in governing the kinetics of fumarate addition. These complexes will be of particular significance while considering the mechanism in the enzyme scenario since it provides a first-hand glimpse into understanding the importance of the hydrogen bonds, non-covalent interactions and other stabilization factors and how they impact the energy landscape for the mechanism. We anticipate that these effects will be important, but their impact on the relative rates will depend on the detailed structure in the enzyme active site. These complexes and transition states for the fumarate addition mechanism form the basis for future hybrid quantum mechanical studies that will incorporate the enzyme structure and evaluate the impact of the protein environment on the fumarate addition mechanism.

5. Acknowledgements.

The authors would like to acknowledge financial support from Dr. David Shifler at the Office of Naval Research, under Award N00014-10-1-0946 and Mr. Kun Wang and Mr. Yogesh Koirala for their helpful discussions during the preparation of the manuscript. Dr. Shubham Vyas gratefully acknowledges the Dreyfus postdoctoral fellowship. The authors would also like to acknowledge support from High Performance Computing and the Golden Energy Computing Organization for access to supercomputing facilities.

Supporting Information. The Mulliken spin density analysis, the kinetic mechanism including all the reactions, A-factors, activation energies and equilibrium constants are provided in the Supplementary Information. This material is available free of charge via the Internet at <http://pubs.acs.org>.

Table of Contents Graphic



References

1. Coschigano, P. W.; Wehrman, T. S.; Young, L. Y., Identification and analysis of genes involved in anaerobic toluene metabolism by strain T1: Putative role of a glycine free radical. *Applied and Environmental Microbiology* 1998, 64, 1650-1656.
2. Van Hamme, J. D.; Singh, A.; Ward, O. P., Recent advances in petroleum microbiology. *Microbiology and Molecular Biology Reviews* 2003, 67, 503-+.
3. Heider, J.; Spormann, A. M.; Beller, H. R.; Widdel, F., Anaerobic bacterial metabolism of hydrocarbons. *Fems Microbiology Reviews* 1998, 22, 459-473.
4. Foght, J., Anaerobic biodegradation of aromatic hydrocarbons: Pathways and prospects. *Journal of Molecular Microbiology and Biotechnology* 2008, 15, 93-120.
5. Mbadinga, S. M.; Wang, L. Y.; Zhou, L.; Liu, J. F.; Gu, J. D.; Mu, B. Z., Microbial communities involved in anaerobic degradation of alkanes. *International Biodeterioration & Biodegradation* 2011, 65, 1-13.
6. Aktas, D. F.; Lee, J. S.; Little, B. J.; Ray, R. I.; Davidova, I. A.; Lyles, C. N.; Sufflita, J. M., Anaerobic Metabolism of Biodiesel and Its Impact on Metal Corrosion. *Energy & Fuels* 2010, 24, 2924-2928.
7. Itah, A. Y.; Brooks, A. A.; Ogar, B. O.; Okure, A. B., Biodegradation of International Jet A-1 Aviation Fuel by Microorganisms Isolated from Aircraft Tank and Joint Hydrant Storage Systems. *Bulletin of Environmental Contamination and Toxicology* 2009, 83, 318-327.
8. Raikos, V.; Vamvakas, S. S.; Sevastos, D.; Kapolos, J.; Karaiskakis, G.; Koliadima, A., Water content, temperature and biocide effects on the growth kinetics of bacteria isolated from JP-8 aviation fuel storage tanks. *Fuel* 2012, 93, 559-566.
9. Widdel, F.; Rabus, R., Anaerobic biodegradation of saturated and aromatic hydrocarbons. *Current Opinion in Biotechnology* 2001, 12, 259-276.
10. Biegert, T.; Fuchs, G.; Heider, F., Evidence that anaerobic oxidation of toluene in the denitrifying bacterium *Thauera aromatica* is initiated by formation of benzylsuccinate from toluene and fumarate. *European Journal of Biochemistry* 1996, 238, 661-668.
11. Grundmann, O.; Behrends, A.; Rabus, R.; Amann, J.; Halder, T.; Heider, J.; Widdel, F., Genes encoding the candidate enzyme for anaerobic activation of n-alkanes in the denitrifying bacterium, strain HxN1. *Environmental Microbiology* 2008, 10, 376-385.
12. Callaghan, A. V.; Davidova, I. A.; Savage-Ashlock, K.; Parisi, V. A.; Gieg, L. M.; Sufflita, J. M.; Kukor, J. J.; Wawrik, B., Diversity of Benzyl- and Alkylsuccinate Synthase Genes in Hydrocarbon-Impacted Environments and Enrichment Cultures. *Environmental Science & Technology* 2010, 44, 7287-7294.
13. Cravo-Laureau, C.; Grossi, V.; Raphel, D.; Matheron, R.; Hirschler-Rea, A., Anaerobic n-alkane metabolism by a sulfate-reducing bacterium, *Desulfatibacillum aliphaticivorans* strain CV2803. *Applied and Environmental Microbiology* 2005, 71, 3458-3467.
14. Callaghan, A. V.; Wawrik, B.; Chadhain, S. M. N.; Young, L. Y.; Zylstra, G. J., Anaerobic alkane-degrading strain AK-01 contains two alkylsuccinate synthase genes. *Biochemical and Biophysical Research Communications* 2008, 366, 142-148.
15. Bharadwaj, V. S.; Dean, A. M.; Maupin, C. M., Insights into the Glycyl Radical Enzyme Active Site of Benzylsuccinate Synthase: A Computational Study. *Journal of the American Chemical Society* 2013, 135, 12279-12288.
16. Funk, M. A.; Judd, E. T.; Marsh, E. N. G.; Elliott, S. J.; Drennan, C. L., Structures of benzylsuccinate synthase elucidate roles of accessory subunits in glycyl radical enzyme activation and activity. *Proceedings of the National Academy of Sciences* 2014.

17. Beller, H. R.; Spormann, A. M., Analysis of the novel benzylsuccinate synthase reaction for anaerobic toluene activation based on structural studies of the product. *Journal of Bacteriology* 1998, 180, 5454-5457.
18. Himo, F., Catalytic mechanism of benzylsuccinate synthase, a theoretical study. *Journal of Physical Chemistry B* 2002, 106, 7688-7692.
19. Arantes, G. M.; Chaimovich, H., Thiolytic and Alcoholysis of Phosphate Tri- and Monoesters with Alkyl and Aryl Leaving Groups. An ab Initio Study in the Gas Phase. *The Journal of Physical Chemistry A* 2005, 109, 5625-5635.
20. Menegon, G.; Loos, M.; Chaimovich, H., Ab Initio Study of the Thiolytic of Trimethyl Phosphate Ester in the Gas Phase. *The Journal of Physical Chemistry A* 2002, 106, 9078-9084.
21. Bruice, T. C.; Lightstone, F. C., Ground State and Transition State Contributions to the Rates of Intramolecular and Enzymatic Reactions. *Accounts of Chemical Research* 1998, 32, 127-136.
22. Jarling, R.; Sadeghi, M.; Drozdowska, M.; Lahme, S.; Buckel, W.; Rabus, R.; Widdel, F.; Golding, B. T.; Wilkes, H., Stereochemical Investigations Reveal the Mechanism of the Bacterial Activation of n-Alkanes without Oxygen. *Angewandte Chemie-International Edition* 2012, 51, 1334-1338.
23. Li, L.; Marsh, E. N. G., Mechanism of benzylsuccinate synthase probed by substrate and isotope exchange. *Journal of the American Chemical Society* 2006, 128, 16056-16057.
24. Hess, R. A.; Hengge, A. C.; Cleland, W. W., Isotope Effects on Enzyme-Catalyzed Acyl Transfer from p-Nitrophenyl Acetate: Concerted Mechanisms and Increased Hyperconjugation in the Transition State. *Journal of the American Chemical Society* 1998, 120, 2703-2709.
25. Himo, F., Stability of protein-bound glyceryl radical: a density functional theory study. *Chemical Physics Letters* 2000, 328, 270-276.
26. Himo, F.; Eriksson, L. A., Catalytic mechanism of pyruvate formate-lyase (PFL). A theoretical study. *Journal of the American Chemical Society* 1998, 120, 11449-11455.
27. Himo, F., C-C bond formation and cleavage in radical enzymes, a theoretical perspective. *Biochimica Et Biophysica Acta-Bioenergetics* 2005, 1707, 24-33.
28. Allemann, R. K.; Young, N. J.; Ma, S.; Truhlar, D. G.; Gao, J., Synthetic Efficiency in Enzyme Mechanisms Involving Carbocations: Aristolochene Synthase. *Journal of the American Chemical Society* 2007, 129, 13008-13013.
29. Booker, S. J., Anaerobic functionalization of unactivated C-H bonds. *Current Opinion in Chemical Biology* 2009, 13, 58-73.
30. Callaghan, A. V., Enzymes involved in the anaerobic oxidation of n-alkanes: from methane to long-chain paraffins. *Frontiers in Microbiology* 2013, 4.
31. Fukui, K., The path of chemical reactions - the IRC approach. *Accounts of Chemical Research* 1981, 14, 363-368.
32. Frisch, M. J.; Trucks, G. W.; Schlegel, H. B.; Scuseria, G. E.; Robb, M. A.; Cheeseman, J. R.; Scalmani, G.; Barone, V.; Mennucci, B.; Petersson, G. A.; Nakatsuji, H.; Caricato, M.; Li, X.; Hratchian, H. P.; Izmaylov, A. F.; Bloino, J.; Zheng, G.; Sonnenberg, J. L.; Hada, M.; Ehara, M.; Toyota, K.; Fukuda, R.; Hasegawa, J.; Ishida, M.; Nakajima, T.; Honda, Y.; Kitao, O.; Nakai, H.; Vreven, T.; Montgomery, J., J. A.; Peralta, J. E.; Ogliaro, F.; Bearpark, M.; Heyd, J. J.; Brothers, E.; Kudin, K. N.; Staroverov, V. N.; Kobayashi, R.; Normand, J.; Raghavachari, K.; Rendell, A.; Burant, J. C.; Iyengar, S. S.; Tomasi, J.; Cossi, M.; Rega, N.; Millam, J. M.; Klene, M.; Knox, J. E.; Cross, J. B.; Bakken, V.; Adamo, C.; Jaramillo, J.; Gomperts, R.; Stratmann, R. E.; Yazyev, O.; Austin, A. J.; Cammi, R.; Pomelli, C.; Ochterski, J. W.; Martin, R. L.;

- Morokuma, K.; Zakrzewski, V. G.; Voth, G. A.; Salvador, P.; Dannenberg, J. J.; Dapprich, S.; Daniels, A. D.; Farkas, Ö.; Foresman, J. B.; Ortiz, J. V.; Cioslowski, J.; Fox, D. J. *Gaussian 09 Rev C.01*, Gaussian, Inc.;
33. Zhao, Y.; Truhlar, D., The M06 suite of density functionals for main group thermochemistry, thermochemical kinetics, noncovalent interactions, excited states, and transition elements: two new functionals and systematic testing of four M06-class functionals and 12 other functionals. *Theoretical Chemistry Accounts* 2008, 120, 215-241.
34. Montgomery, J. A.; Frisch, M. J.; Ochterski, J. W.; Petersson, G. A., A complete basis set model chemistry. VI. Use of density functional geometries and frequencies. *Journal of Chemical Physics* 1999, 110, 2822-2827.
35. Zhao, Y.; Truhlar, D. G., Density Functionals with Broad Applicability in Chemistry. *Accounts of Chemical Research* 2008, 41, 157-167.
36. Hohenstein, E. G.; Chill, S. T.; Sherrill, C. D., Assessment of the Performance of the M05-2X and M06-2X Exchange-Correlation Functionals for Noncovalent Interactions in Biomolecules. *Journal of Chemical Theory and Computation* 2008, 4, 1996-2000.
37. Zheng, J.; Zhao, Y.; Truhlar, D. G., The DBH24/08 Database and Its Use to Assess Electronic Structure Model Chemistries for Chemical Reaction Barrier Heights. *Journal of Chemical Theory and Computation* 2009, 5, 808-821.
38. Zhao, Y.; Truhlar, D. G., How Well Can New-Generation Density Functionals Describe the Energetics of Bond-Dissociation Reactions Producing Radicals? *The Journal of Physical Chemistry A* 2008, 112, 1095-1099.
39. Thanthiriwatt, K. S.; Hohenstein, E. G.; Burns, L. A.; Sherrill, C. D., Assessment of the Performance of DFT and DFT-D Methods for Describing Distance Dependence of Hydrogen-Bonded Interactions. *Journal of Chemical Theory and Computation* 2010, 7, 88-96.
40. Tishchenko, O.; Zheng, J.; Truhlar, D. G., Multireference Model Chemistries for Thermochemical Kinetics. *Journal of Chemical Theory and Computation* 2008, 4, 1208-1219.
41. Xu, X.; Alecu, I. M.; Truhlar, D. G., How Well Can Modern Density Functionals Predict Internuclear Distances at Transition States? *Journal of Chemical Theory and Computation* 2011, 7, 1667-1676.
42. Zheng, J.; Zhao, Y.; Truhlar, D. G., Thermochemical Kinetics of Hydrogen-Atom Transfers between Methyl, Methane, Ethynyl, Ethyne, and Hydrogen. *The Journal of Physical Chemistry A* 2007, 111, 4632-4642.
43. Zhang, F.; Dibble, T. S., Impact of tunneling on hydrogen-migration of the n-propylperoxy radical. *Physical Chemistry Chemical Physics* 2011, 13, 17969-17977.
44. *CHEMKIN-PRO*, 15131; Reaction Design: San Diego, 2013.
45. Blanksby, S. J.; Ellison, G. B., Bond Dissociation Energies of Organic Molecules. *Accounts of Chemical Research* 2003, 36, 255-263.
46. Sabbe, M. K.; Reyniers, M.-F.; Van Speybroeck, V.; Waroquier, M.; Marin, G. B., Carbon-Centered Radical Addition and β -Scission Reactions: Modeling of Activation Energies and Pre-exponential Factors. *ChemPhysChem* 2008, 9, 124-140.
47. Li, L.; Marsh, E. N. G., Deuterium isotope effects in the unusual addition of toluene to fumarate catalyzed by benzylsuccinate synthase. *Biochemistry* 2006, 45, 13932-13938.
48. Yang, Y.; Liu, L.; Chen, J.; Han, K., Hydrogen bonding tunes the early stage of hydrogen-atom abstracting reaction. *Physical Chemistry Chemical Physics* 2014, 16, 17828-17834.

49. Qiao, C. H.; Marsh, E. N. G., Mechanism of benzylsuccinate synthase: Stereochemistry of toluene addition to fumarate and maleate. *Journal of the American Chemical Society* 2005, 127, 8608-8609.